Surfaces and Interfaces 44 (2024) 103671

Contents lists available at ScienceDirect

Surfaces and Interfaces

journal homepage: www.sciencedirect.com/journal/surfaces-and-interfaces

One and two-step electrodeposition of composite films of calcium-deficient hydroxyapatite matrix with nanoscale Ag- and Zn-based particles

Michael Escobar [a], Volker Hoffmann [b], Thomas Gemming [b], Minsoo Kim [c], Salvador Pané [c], Jordi Sort [a,d], Eva Pellicer [a,*]

[a] Departament de Física, Universitat Autònoma de Barcelona, Cerdanyola del Vallès, Bellaterra 08193, Spain
[b] Leibniz Institute for Solid State and Materials Research, Helmholtzstr. 20, Dresden D-01069, Germany
[c] Institute of Robotics and Intelligent Systems, ETH Zurich, Tannenstrasse 3, Zurich 8092, Switzerland
[d] Institució Catalana de Recerca i Estudis Avançats (ICREA), Pg. Lluís Companys 23, Barcelona 08010, Spain

ARTICLE INFO

Keywords:
Surface modification
Electrodeposition
Composite coatings
Hydroxyapatite
Metallic nanoparticles
Characterization

ABSTRACT

A fundamental study regarding the electrochemical synthesis of composite coatings with application in the orthopaedic field has been conducted. In particular, the electrodeposition of calcium phosphate coatings with Ag nanoparticles (AgNPs) from either a single electrolyte (one-step, 1S) or two electrolytes (two-step, 2S) on a β-Ti alloy (Ti-18Mo-6Nb-4Ta in wt%) was investigated. Pulse current deposition was implemented to produce the composite coatings by the 1S approach from a simple solution containing 42 mM $Ca(NO_3)_2{\cdot}4H_2O$, 25 mM $NH_4H_2PO_4$, and 0.5 mM $AgNO_3$ at 65°C. Meanwhile, the calcium phosphate matrix was also deposited by pulse current, and Ag was afterwards grown by direct current from 0.1 M KNO_3 + x mM $AgNO_3$ (x = 5, 10) at 25 °C (2S approach). The Ca/P ratio of the matrix was compatible with the formation of calcium-deficient hydroxyapatite (CDHA). The resulting Ag content in the composites could be varied between 4 and 13 wt% as a function of the working conditions. The 2S-derived coatings produced by electroplating Ag at j = –20.8 mA/cm^2 from 0.1 M KNO_3 + 10 mM $AgNO_3$ furnished an optimal dispersion of the AgNPs on top of the CDHA matrix, while aggregation and/or dendritic growth was observed in other cases. Glow discharge optical emission spectrometry (GDOES) measurements indicated that a given amount of AgNPs becomes engulfed in the CDHA matrix during the 1S electrodeposition, whereas most of them decorate its outer surface in the 2S-derived coatings. The applicability of the two approaches was extended to the case of zinc oxide. ZnO-containing CDHA coatings in which the Zn element was homogeneously distributed across the film surface were obtained from 42 mM $Ca(NO_3)_2{\cdot}4H_2O$, 25 mM $NH_4H_2PO_4$ and 1 mM $Zn(NO_3)_2{\cdot}6H_2O$ at 65 °C (1S approach). On the contrary, ZnO-NPs could be clearly observed when deposition from 5 mM KNO_3 + 5 mM $Zn(NO_3)_2$ was performed at 70 °C on top of previously grown CDHA (2S approach). The results indicated that the percentage and location of the antibacterial element (Ag, Zn) in the calcium phosphate matrix can be tuned on demand to a great extent by electrochemical means.

1. Introduction

The main goal behind the synthesis of composite coatings is to achieve better (and often synergetic) properties than those of the individual components alone by the combination of two or more materials in the same coating. Composite coatings can be manufactured by different methods such as chemical vapour deposition, plasma and thermal spraying, dipping, micro-arc oxidation, sol-gel, electrodeposition, or electrophoretic deposition [1–4]. Among them, electrodeposition shows several advantages including low cost, the possibility to produce structural features with sizes ranging from nm to μm, relatively high deposition rates, strong adhesion between the coating and the substrate, uniformity of deposition over complex shaped substrates, reduction of waste compared to dipping or spraying techniques, and the possibility for rapid scale-up to an industrial setting [5].

Metal matrix – nanosized ceramic particle composites are the most common composites obtained by electrodeposition [6]. Typically, the ceramic nanoparticles (NPs) are suspended in an electrolyte containing

* Corresponding author.
E-mail address: eva.pellicer@uab.cat (E. Pellicer).

https://doi.org/10.1016/j.surfin.2023.103671
Received 14 September 2023; Received in revised form 8 November 2023; Accepted 22 November 2023
Available online 23 November 2023

the metal precursors and the particles become embedded in the growing metal coating. Ceramic matrix – metal particle and ceramic matrix – ceramic particle composites are also available by electrochemical means although the related literature is more limited. Most of the examples of ceramic matrix composites refer to calcium phosphate. In this case, the deposition of the calcium phosphate host takes place when suitable conditions for the electroreduction of water, protons or other species (e.g., NO_3^{2-} or O_2^-) are set in the electrolyte upon the application of a potential or current density. Under this scenario, calcium phosphate can precipitate onto the substrate from their corresponding precursors, which are typically calcium nitrate tetrahydrate ($Ca(NO_3)_2{\cdot}4H_2O$) and ammonium dihydrogen phosphate ($NH_4H_2PO_4$) [7].

The deposition of calcium phosphate coatings (often referred to as CaP for simplicity) on titanium (Ti) alloys has been widely researched for applications in the orthopaedic and dentistry fields [8]. The family of CaP compounds is rather rich, being hydroxyapatite (HA) with the chemical formula $Ca_{10}(PO_4)_6(OH)_2$ the archetypical one because of its chemical and structural similarity to human bone. In this line, there is quite a large body of literature regarding the production of stoichiometric and non-stoichiometric hydroxyapatite (HA) on Ti-based substrates by electrochemical means [9–11]. However, CaP coatings alone might not endow a biomaterial with all the requirements for implantology. The need to prevent biofilm formation on the implant surface and, hence, overcome implant related infections, has become a serious concern [12]. For this reason, elements or compounds exhibiting antibacterial properties, such as Ag, ZnO, and Cu have been added to HA, often in the form on NPs [13–15]. Of them, HA-Ag composites are the most widely investigated so far.

HA-Ag composites have been prepared by both one step and two-step electrodeposition. For example, Lu et al. [16] applied potentiostatic pulse deposition ($-E_c$ = 1.3 – 4.0 V) to produce HA-Ag nanoparticle (HA-AgNP) films on commercial pure (CP) Ti substrates from an electrolyte containing 5 mM $Ca(NO_3)_2$, 3mM $NH_4H_2PO_4$, cysteine, and varying $AgNO_3$ concentrations (0.5 – 1 mM) at 40 °C. Following electrodeposition, the samples were heat-treated at high temperature to improve the adhesive strength. The resulting Ag content, determined by energy dispersive X-ray spectroscopy (EDX), was between 7 and 15 wt%, and an antibacterial effect was observed. However, the elements considered in the EDX analysis for the quantification of Ag are not specifically mentioned in this study. Similarly, Xie et al. [17] prepared HA-AgNPs coatings from a single electrolyte by potentiostatic pulse deposition at E_c = –1.3 V with a pulse duration of 100 s for 1 h. On the other hand, the decoration of previously grown HA coating with AgNPs using potentiostatic approaches from a high temperature electrolyte has been typically targeted. In the study by Fu et al. [18] HA was first deposited under DC galvanostatic electrodeposition at a relatively high temperature (95°C) during 2 min onto CP Ti substrates. Followed by this, Ag was deposited on the HA-coated Ti from an electrolyte containing NaCl and $AgNO_3$ also under DC and at the same high temperature as the previous step. The Ag content in the composite samples obtained after electrodeposition of Ag on top of HA at –12.5 mA/cm^2 for 90 s was 7 wt%, as estimated by EDX from considering O, P, Ca, Ag, and Ti elements. Importantly, the Ca/P reported in this study was 1.09, which is much below that of stoichiometric HA (1.67), and even below the threshold value for calcium-deficient hydroxyapatite (CDHA). In another study, a CaP coating was first grown on Ti substrates followed by the potentiostatic deposition of AgNPs at –1.4 V for 6 min at 95°C from a solution containing NaCl and $AgNO_3$ [13]. The deposition of AgNPs on top of HA coated on orthodontic mini-screws was also performed from an electrolyte that contained just $AgNO_3$ at 95°C with a constant potential of –2.5 V during 3 min [19]. Other approaches have been also pursued, like immersing the as-electrodeposited HA coating in a suspension of AgNPs to facilitate its incorporation into the coating [20].

In the case of Zn, studies dealing with the incorporation of ZnO particles in CaP coatings by electrochemical means are scarcer. Mehrvarz et al. [21] used an electrolyte containing $Ca(NO_3)_2{\cdot}4H_2O$, $NH_4H_2PO_4$ and $NaNO_3$ to which pre-formed ZnO NPs were suspended to the electrolyte. Deposition on a NiTi substrate was done in cathodic pulses of –6 mA/cm^2 with t_{on} and t_{off} of 1 and 9 s, respectively, for 30 min at 65°C. A similar approach was utilized by Huang et al. to produce Sr-doped HA coating containing ZnO [22]. However, although ZnO was homogeneously distributed in the coating, it was not in the form of well-defined NPs. Indeed, most of the times, Zn has been incorporated in the calcium phosphate coatings as a dopant. Recently, Maimaiti et al. showed the electrochemical manufacturing of HA/polypyrrole/ZnO-NPs composite coatings from an electrolyte containing $ZnNO_3$ as a precursor [14].

The objective of the present study is to fabricate a composite coating made of CDHA and AgNPs on top of a previously developed β-type TiMoNbTa alloy [23]. As opposed to other studies, no pre-formed AgNPs, nor coordination agents/stabilizers in the electrolyte, and mild working conditions of temperature were employed. Two different approaches were used, namely, a one-step method where the NPs and CDHA are deposited simultaneously; and a two-step method consisting in the decoration of previously electrodeposited CDHA coating with the AgNPs. The approaches were extended to the ZnO case, showing the occurrence of ZnO NPs populating the surface of the coatings produced by the two-step method.

2. Material and methods

2.1. Electrochemical synthesis of the composites

For the electrodeposition, disks of a β-Ti alloy were used as substrate. The Ti alloy composition consisted of Ti-18Mo-6Nb-4Ta (wt%) and it was fabricated following the same process as reported in a previous study [23]. Briefly, pieces of Ti, Mo, Nb and Ta, with weights corresponding to the established formulation, were placed in a mini arc-melting system (MAM-1) and then melted until a homogeneous blend was obtained. Then, a rod was made out of the blend by suction casting in a copper mold with a 4 mm diameter. The rod was cut into 2.5 mm thick disks and they were polished with SiC papers up to 4000 grit. To provide electrical contact to the disks, they were grabbed from their side with a metallic tweezer/pen and wrapped with Teflon tape for isolation, leaving the polished surface unwrapped in order to coat it by electrodeposition. The electrodeposition processes were conducted on an electrolytic cell with a platinum wire as a counter electrode, a double junction Ag/AgCl with 0.5 M KNO_3 outer solution and 3 M KCl inner solution as a reference electrode, and the Ti alloy disk as a working electrode. The electrodes were connected to an Autolab PGSTAT302N potentiostat/galvanostat. The temperature of the cell was kept constant with the aid of a thermostat jacket with a heating circulator (Julabo F12).

Prior to the growth of the composite coatings, the electrolytes were characterized by linear sweep voltammetry (LSV) and cyclic voltammetry (CV). Notably, this type of more fundamental studies is rather scarce in literature since the focus is typically laid on the biological properties of the resulting coatings. The potential was first swept towards cathodic values, starting from a potential at which no current was recorded, at a scan rate of 50 mV/s. Glassy carbon rod of 2 mm in diameter and the β-Ti alloy disks were used as working electrodes. The glassy carbon surface was wet polished with alumina of 0.3 μm diameter and ultrasonically cleaned in water. The working temperature was the same as that applied for the subsequent growth of the coatings, i.e., 65°C for the electrolytes used for the simultaneous electrodeposition of both CDHA/Ag- or ZnO-NPs, and 25 and 70°C for the electrolytes used for the electrodeposition of Ag- and ZnO-NPs over the substrate previously coated with CDHA, respectively.

For the one-step electrodeposition (1S-ED), the precursors for the calcium deficient hydroxyapatite (CDHA), as well as for the silver nanoparticles (AgNPs) were all within the electrolyte solution; thus, the

electrolyte consisted of 100 mL of a solution containing 42 mM Ca $(NO_3)_2{\cdot}4H_2O$, 25 mM $NH_4H_2PO_4$ and 0.5 mM $AgNO_3$ that was kept at 65°C. Different average current densities (j_c) were applied with fixed t_{on} of 1 s and varying t_{off}. 184 cycles were used in all cases, which lead to an overall charge density of –0.98 C/cm^2. The average current densities (with their corresponding t_{off}) were as follows: –1.3 mA/cm^2 (3 s), –1.8 mA/cm^2 (2 s) and –2.7 mA/cm^2 (1 s). A second batch of samples were produced with the same parameters, and immediately following electrodeposition, they were subjected to a post-treatment by immersing them in 0.1 M NaOH during 48 h. Such alkaline post-treatment increases the pH and provides sufficient OH^- ions to react with Ca^{2+} and PO_4^{3-} released from the as-deposited calcium phosphate during immersion, promoting the redeposition and stabilization of the desired CDHA phase [24]. Once the coatings were produced, with and without alkaline post-treatment (Fig. 1a), the samples were rinsed in ultra-pure water several times to remove any unreacted reagents and then they were left to dry in air for future characterizations.

In the case of the two-step electrodeposition (2S-ED), the substrates were first coated with CDHA from the same electrolyte as for 1S-ED but without the $AgNO_3$ salt [23]. The electrodeposition process was performed in a pulsed current fashion as well. In this case, an average current density of –1.8 mA/cm^2 was applied with $t_{on} = 1$ s and $t_{off} = 2$ s during 167 cycles, resulting in an overall charge density of –0.89 C/cm^2. After this, the samples were immersed in NaOH 0.1 M during 48 h, rinsed with ultra-pure water and dried in air. Subsequently, a second electrodeposition step was performed on the samples under direct current (DC) galvanostatic conditions using 100 mL of an electrolyte containing 0.1 M KNO_3 plus 5 mM or 10 mM $AgNO_3$ at 25°C (Fig. 1b). The applied current densities were –10.6, –20.8 and –42.4 mA/cm^2 (for 180, 92 and 45 s, respectively, to maintain a charge density of –1.91 C/cm^2). Note that the two methods were performed in a galvanostatic fashion by varying the pulse current densities applied, as opposed to the commonly reported potentiostatic deposition of Ag.

To assess the validity of the approaches to other metal-containing CDHA composites, attempts were made to produce composites consisting of CDHA matrix and ZnO-NPs on the same β-Ti alloy. For the 1S-ED, the electrolyte was 100 mL of a solution containing 42 mM Ca $(NO_3)_2{\cdot}4H_2O$, 25 mM $NH_4H_2PO_4$ and 1 mM $Zn(NO_3)_2{\cdot}6H_2O$ that was kept at 65°C. Here, the j_c (and the number of cycles) for the pulse were –1.3 (367), –2.7 (177) and –5.4 (88) mA/cm^2 with both t_{on} and t_{off} of 1 s, to ultimately apply a charge density of –0.92 C/cm^2. Similarly, the 2S-ED was also used to obtain nanoscale ZnO on top of CDHA that was previously deposited with the same procedure as described above. For this, 100 mL of an electrolyte containing 5 mM $Zn(NO_3)_2{\cdot}6H_2O$ and 5 mM KNO_3 at 70°C was used. The applied current densities were –1, –2.2 and –4.4 mA/cm^2 (for 1781, 809 and 405 s, respectively, to maintain a charge density of –1.78 C/cm^2).

2.2. Characterization of the composites

The morphology and the chemical composition of the produced coatings were investigated through field-emission scanning electron microscopy (FESEM) on a Zeiss Merlin equipped with energy-dispersive X-ray (EDX) spectroscopy and electron backscattered (EBS) detectors. EDX was performed on five different areas of each coating at a magnification of 1000x with an applied voltage of 15 kV. The mean values are reported here with their corresponding error. The Ag percentage in the coatings was determined by considering Ca, P and Ag elements while disregarding the rest, unless otherwise stated. Similarly, the Zn percentage in the Zn-containing coatings was determined by considering Ca, P and Zn elements.

The roughness of the as-polished b-Ti substrate was measured on an optical profilometer Leica DCM 3D. The root mean square roughness (R_q) value was determined from different areas and it is reported as mean value ± standard deviation. The thickness of the Ag-containing composite coatings was assessed with cuts done with the focused ion beam (FIB) technique (FIB, Helios 5 CX, Thermo Fisher Scientific, Waltham, MA, USA) and images of the coatings' cross-sections were acquired by SEM with an ion conversion and electron (ICE) detector at 5 kV acceleration voltage. Meanwhile, the thickness of the Zn-containing composite coatings was assessed with the focused ion beam (FIB, Helios 5 UX, Thermo Fisher Scientific, USA), cutting using Ga-ion at 30 kV (starting current at 1.2 nA and finishing at 90 pA). The cross-section images of the coating were acquired with an ion conversion and electron (ICE) detector at 2 kV acceleration voltage.

Glow discharge optical emission spectrometry (GDOES) analyses were performed on a GDA750 HR (Spectruma, Germany). The samples were positioned on a 0.2 mm thick Al_2O_3 plate with a 1 mm hole in the radio-frequency mode with back coupling of the rf voltage. A 1.6 mm anode diameter was used. Moderate sputtering conditions were selected in order to avoid thermal problems, where the layer is removed from the substrate and sparking appears. The selected conditions were 500 V anode voltage at the free running tube generator and 2.1 hPa. Ti, Ca, P and Ag were measured at wavelengths of 399.864, 393.367, 177.499

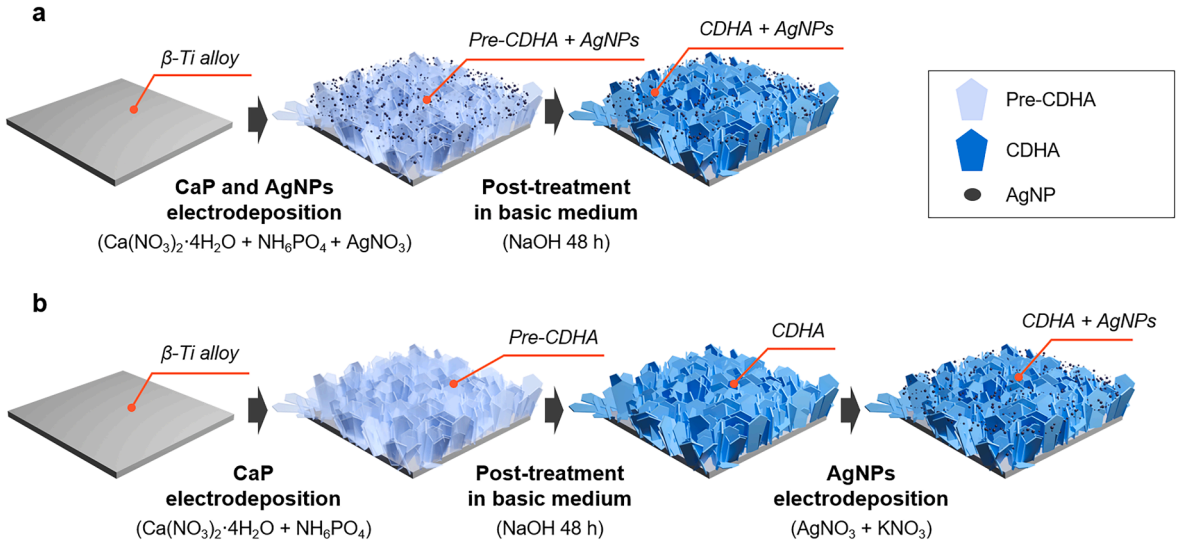

Fig. 1. Diagram depicting the (a) 1S- and (b) 2S-ED processes for coating the β-Ti alloy with a composite film consisting of calcium-deficient hydroxyapatite (CDHA) matrix and silver nanoparticles (AgNPs).

and 338.289 nm, respectively, with photomultipliers in the polychromator optics at the highest amplification (about 1000 V).

The crystallographic structure of the coatings was analysed by grazing incidence X-ray diffraction (GIXRD). The patterns were acquired on a Bruker D8-Discover diffractometer with Cu K_α radiation (λ = 1.5406 Å) in the range of 20 – 90° at an incidence angle of 0.9°, and a step size of 0.020°. The ICDD PDF2 database was used for phase identification.

3. Results and discussion

Fig. 1 shows a schematic diagram of the two approaches followed to obtain the CaP-based composites. The selection of the working conditions to grow the different composite components was based on prior literature [23,25,26] and the data gleaned from LSV and CV curves (as shown below).

Fig. 2 shows the LSV and CV curves obtained from the Ca $(NO_3)_2.4H_2O$ + 25 mM $NH_4H_2PO_4$ + 0.5 mM $AgNO_3$ electrolyte at 65 °C. The green LSV (curve *i*) shows some reduction waves in the positive potential range, being a small reduction peak centered at +0.15 V the most notable feature (see inset). Two consecutive waves are recorded further at negative potentials, between –0.7 V and –1.1 V. The cathodic branch of the CV recorded on glassy carbon from the same electrolyte shows similar features, although the two waves previously recorded at negative potentials merge into a single reduction peak (curve *ii*). It was conjectured that the reduction current placed at positive potentials corresponded to the reduction of Ag^+ ions to metallic silver. To verify this hypothesis, the fingerprint of a blank solution containing 10 mM $AgNO_3$ + 0.1 M KNO_3 was captured [26]. Curves *iii* and *iv* recorded on the β-Ti alloy and the glassy carbon electrodes, respectively, indeed show the occurrence of reduction waves of higher intensity in the same window of positive potentials. The anodic branch of the CV recorded on the glassy carbon shows an anodic peak attributed to the stripping of the silver previously deposited during the cathodic sweep [26]. The absence of an Ag-related stripping peak in curve *ii* is attributed to the much lower amount of Ag deposited in this case during the cathodic sweep. According to the information gathered from the LSVs and CVs, average current densities between –1.3 and –2.7 mA cm^{-2} were selected to achieve the conditions suitable for both the precipitation of CaP and the reduction of Ag^+ ions into the same coating (1S-ED). Note that the deposition of CaP alone onto the same β-alloy was proven feasible in the range of j_c between –1.8 and –8.2 mA cm^{-2} [23].

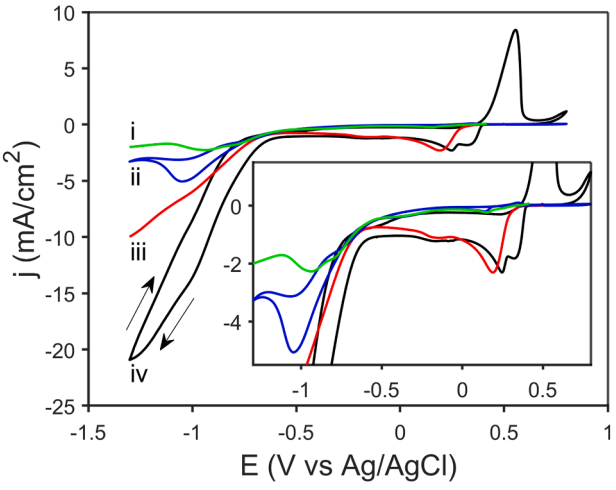

Fig. 2. (i) Linear sweep voltammetry (LSV) on Ti-18Mo-6Nb-5Ta substrate and (ii) cyclic voltammetry (CV) on glassy carbon from 42 mM $Ca(NO_3)_2{\cdot}4H_2O$ + 25 mM $NH_4H_2PO_4$ + 0.5 mM $AgNO_3$, (iii) LSV on Ti-18Mo-6Nb-5Ta substrate and (iv) CV on glassy carbon from 10 mM $AgNO_3$ + 0.1 M KNO_3. Scan rate: 50 mV/s.

The chemical composition of the coatings produced from the 1S-ED and 2S-ED approaches were studied by EDX (Fig. 3). A representative pattern of a composite coating obtained by 1S-ED is shown in Fig. 3a. The presence of the elements originating from the Ti alloy substrate (Ti, Mo, Nb, and Ta), Ca and P from the CDHA matrix, and Ag from the secondary phase is verified. Fig. 3b shows the Ca/P ratio determined on coatings obtained at varying current densities, in which a slight increase of this ratio was observed after subjecting the coatings to a post-alkaline treatment, in agreement with previous studies [24]. Yet, the Ca/P ratios after the treatment with NaOH did not increase as expected, suggesting that the presence of Ag in the coatings is impacting the chemical composition of the CaP matrix in some way. The Ag percentage in the coatings before the alkaline post-treatment was around 4-5 wt% independently of the average current density (Fig. 3c). The percentage of Ag increased to 7 - 10 wt% after immersion of the coatings in NaOH. This result can be explained by the fact that oxygen is not considered in the EDX quantification. If Ca, P, Ag and O elements are considered, then the resulting Ag percentage remains constant at 3 ± 1 wt% both before and after the NaOH treatment.

A representative EDX pattern of a composite coating produced from 2S-ED is shown in Fig. 3d, which shows a relative higher amount of Ag compared to that of Fig. 3a. The Na signal originates from a remanent of the alkaline treatment applied right after CaP deposition. The Ca/P ratios detected in the 2S-ED derived coatings are shown in Fig. 3e. In this case, the alkaline post-treatment was applied before the electrodeposition of Ag and, therefore, the Ca/P ratios already correspond to alkaline-treated calcium phosphate. Here, the x-axis corresponds to the DC current density applied for the electrodeposition of Ag on top of the previously deposited CDHA. Notice that Ag could be deposited onto the CDHA coating in spite of its low electrical conductivity. The effect of the processing route and the working parameters have shown to play a substantial role in tailoring the conductivity of ceramic materials. For example, Horiuchi et al. found that HA consists of conductive grains and insulating grain boundaries [27]. In our study, we confirm that the CDHA can be negatively polarized and induce the discharge of Ag ions on its rough surface, in agreement with previous studies [13,18,19]. Sufficiently negative current densities in the range between –10 and –42 mA/cm^2 were applied for this purpose, which are the values depicted in the x-axis. As expected, the Ca/P ratio remained the same independently of both the $AgNO_3$ concentration in the second electrolyte and the applied *j*. Instead, the Ag wt% was significantly different in coatings obtained from 5 mM and 10 mM $AgNO_3$ solutions except for the more negative *j* applied. In particular, the amount of Ag in the composite coatings raised from 4 wt% to 11-13 wt% when *j* was decreased from –10.6 to –20.8 mA/cm^2.

SEM images of the morphology of composite coatings produced by the two different methods are shown in Fig. 4. In general, for the 1S-ED approach, the CDHA component, characterized by a leaf-like morphology, is very much visible on the surface of the β-Ti alloy. However, at some spots, engulfed in the CDHA matrix, aggregates of submicron particles of rounded shape can be distinguished (Fig. 4a, b). These bunches of particles, which grow in a dendritic fashion, are attributed to Ag and have been previously observed [25]. The formation of these dendritic structures is associated to the sufficiently negative overpotential achieved during the peak pulse current densities and the absence of stabilizing agents in the electrolyte. Noteworthily, composite deposits grown by 1S-ED approach from an electrolyte containing 1 mM $AgNO_3$ gave rise to coatings with larger amounts of Ag, in excess of 15 wt%. In addition, the dendritic growth of Ag was far more evident, giving rise to large aggregates (Fig. S1, Supplementary information).

On the other hand, the coatings resulting from the 2S-ED approach (Fig. 4c, d) show the entire uppermost part of the CDHA matrix completely covered with AgNPs, which have a good dispersion and exhibit lower agglomeration degree compared to the NPs from the 1S-ED method derived coatings. The average size of the AgNPs deposited from 0.1 M KNO_3 + 5 mM $AgNO_3$ at j = –20.8 mA/cm^2 (Fig. 4c) is 52 ± 41

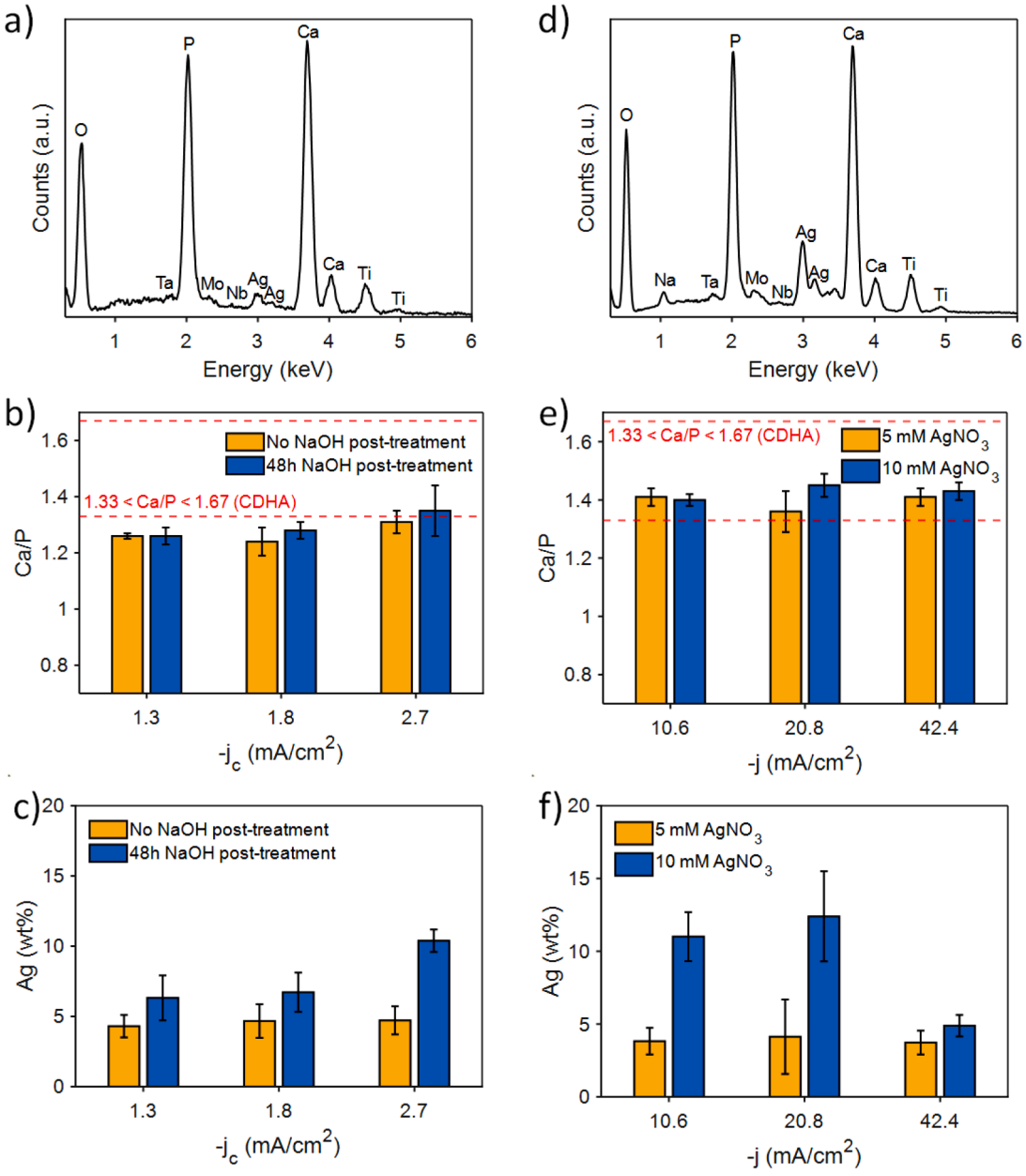

Fig. 3. Compositional analysis of (a-c) coatings obtained by 1S-ED approach: (a) Representative EDX pattern of a coating produced at $j_c = -2.7$ mA/cm^2 followed by NaOH treatment, (b) Ca/P ratio and (c) wt% Ag in coatings produced at the indicated j_c both before and after the NaOH treatment. Compositional analysis of (d-f) coatings obtained by 2S-ED approach: (d) Representative EDX pattern of a coating obtained by CDHA deposition followed by NaOH treatment and finally Ag deposition from 10 mM $AgNO_3$ at $j = -20.8$ mA/cm^2, (e) Ca/P ratio and (f) wt% Ag in coatings produced at the indicated j and precursor concentration for Ag deposition on top of the CDHA.

nm. Meanwhile, that of the particles deposited at the same *j* but from 0.1 M KNO_3 + 10 mM $AgNO_3$ (Fig. 4d) is 74 ± 37 nm. Fig. 4e and f show the SEM and EBS image of the same coating shown in panel *c* but at a lower magnification. The very tiny bright spots in the EBS image confirm the presence of highly dispersed AgNPs, which was achieved without the addition of stabilizing agents in the electrolyte. Indeed, these are rather optimal conditions for the growth of CDHA-AgNPs composites. The corresponding E-t curves recorded during the deposition of Ag on the CDHA-coated β-Ti alloy are shown in Fig. S2, Supplementary Information. The adhesion of 1S-ED and 2S-ED coatings was similar. The R_q for the as-polished β-Ti alloy was 142 ± 20 nm, as measured from optical profilometry.

The XRD patterns of two representative coatings obtained from the 1S- and 2S-ED approaches are shown in Fig. 5a. Besides the peaks ascribed to the β-phase of Ti (PDF 044-1288) substrate, peaks originating from the CDHA (PDF 009-0432) matrix are visible in both cases. For the 1S-ED derived coating, the presence of reflections arising from the Ag species was not obvious, likely because its amount is below the detection limit of the XRD technique (usually taken as 2 wt%). Recall that the Ag quantification by EDX only considered Ca, P and Ag elements. For the 2S-ED derived coating, a weak peak at 45° matching the (200) face-centered cubic (fcc) phase of Ag (PDF 087-0719) was detected (Fig. 5a). Notice that the (111) reflection of fcc-Ag at 38.3° overlaps with the most intense of β-Ti phase, which precludes a clear-cut identification. Also, the presence of oxidized Ag species (labelled as 'Ag ox' in the XRD pattern) could not be ruled out, which can be partly attributed to the alkaline treatment applied to increase the Ca/P ratio of the as-deposited CaP matrix.

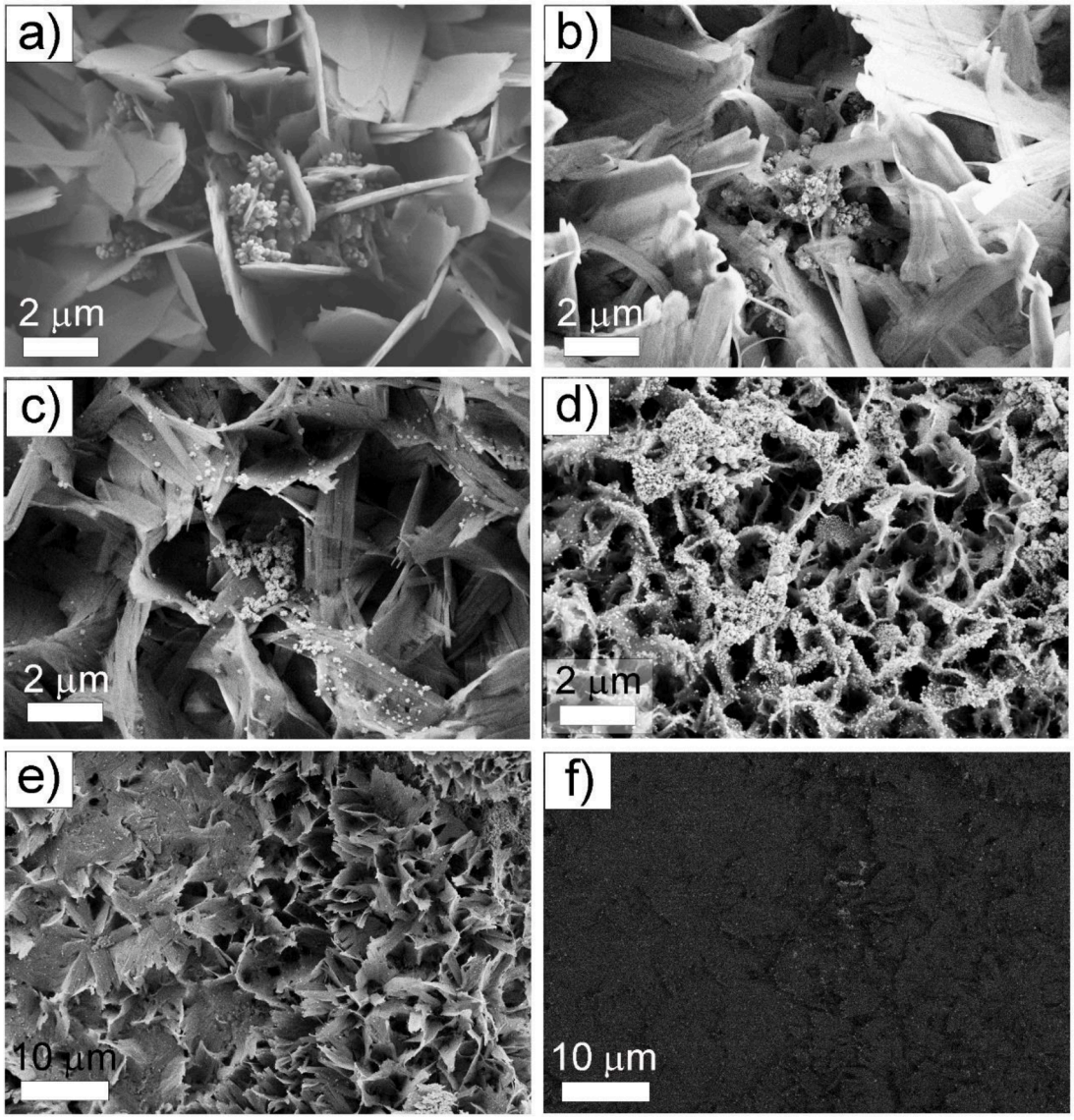

Fig. 4. SEM images of composite coatings obtained by 1S-ED approach at (a) $j_c = -1.3$ mA/cm^2 and (b) $j_c = -2.7$ mA/cm^2, in both cases followed by NaOH treatment; 2S-ED approach at (c) $j = -20.8$ mA/cm^2 from 5 mM $AgNO_3$ and (d) $j = -20.8$ mA/cm^2 from 10 mM $AgNO_3$; e) and f) are the SEM and corresponding electron backscattered (EBS) images of a composite also obtained by the 2S-ED approach at (c) $j = -20.8$ mA/cm^2 from 5 mM $AgNO_3$ in which the bright tiny spots in the EBS image correspond to the AgNPs.

Cross-sections of selected composite coatings obtained from 1S- and 2S-ED approaches were prepared and the intensity-time profiles of Ag, Ca, P, and Ti elements were generated by GDOES (Fig. 5b and c, respectively). In the case of the 1S-ED (Fig. 5b), clearly in the first 12 s there is a Ca and P rich layer sputtered alongside some Ag signal that decays gradually with time. After 12 s, the Ag intensity shows a small increase and a signal corresponding to the Ti based substrate starts to become dominant. Most probably, the sputtering crater reached the substrate after 12 s and started to preferentially sputter the conductive material in the surroundings, i.e. the Ag. After 20 s, the remaining part of the non-conductive surface layer (Ca and P) is quickly removed by sputtering and the substrate signals reach their bulk value. The small increase of the Ag signal at 12 s is most probably caused by crater edge effects at the transition between non-conductive layer and the conductive substrate [28]. For the 2S-ED (Fig. 5c), again there is a Ca and P rich region on top for about 12 s, followed by the increase of the signal belonging to the substrate to the bulk values. However, at the very beginning of the sputtering time the intensity of the Ag signal is significantly higher than for the 1S-ED method, and in this case, it decreases rapidly during the first 3 s. This would confirm that the coatings produced by the 2S-ED method are more enriched in Ag at the surface and that Ag preferentially lies on top of the CDHA matrix, while for those produced with the 1S-ED method the Ag is more distributed within and along the CDHA matrix till the interface with the substrate. The cross-section images shown as insets in Fig. 5b and c show that the 2S-ED coating is thinner than its 1S-ED counterpart (1.4 mm versus 4.7 mm, respectively). The 1S-ED approach gave rise to a more open (i.e., more porous) coating, whilst the 2S-ED derived coatings were denser and, hence thinner, since CDHA was first deposited without the disturbance of Ag^+ ions discharge.

In order to extend the validity of the galvanostatic 1S- and 2S-ED methods to other antibacterial elements, the growth of CDHA coatings with ZnO-NPs was attempted. Fig. 6 shows the combined LSV and CV study of the electrolyte solutions employed for their electrosynthesis. The comparison between *i* and *ii* curves does not provide significant information regarding the codeposition of Zn species and CaP. Instead, the response of a reference electrolyte (5 mM $Zn(NO_3)_2{\cdot}6H_2O$ + 5 mM KNO_3) on the glassy carbon electrode (curve *iv*) shows a nucleation loop

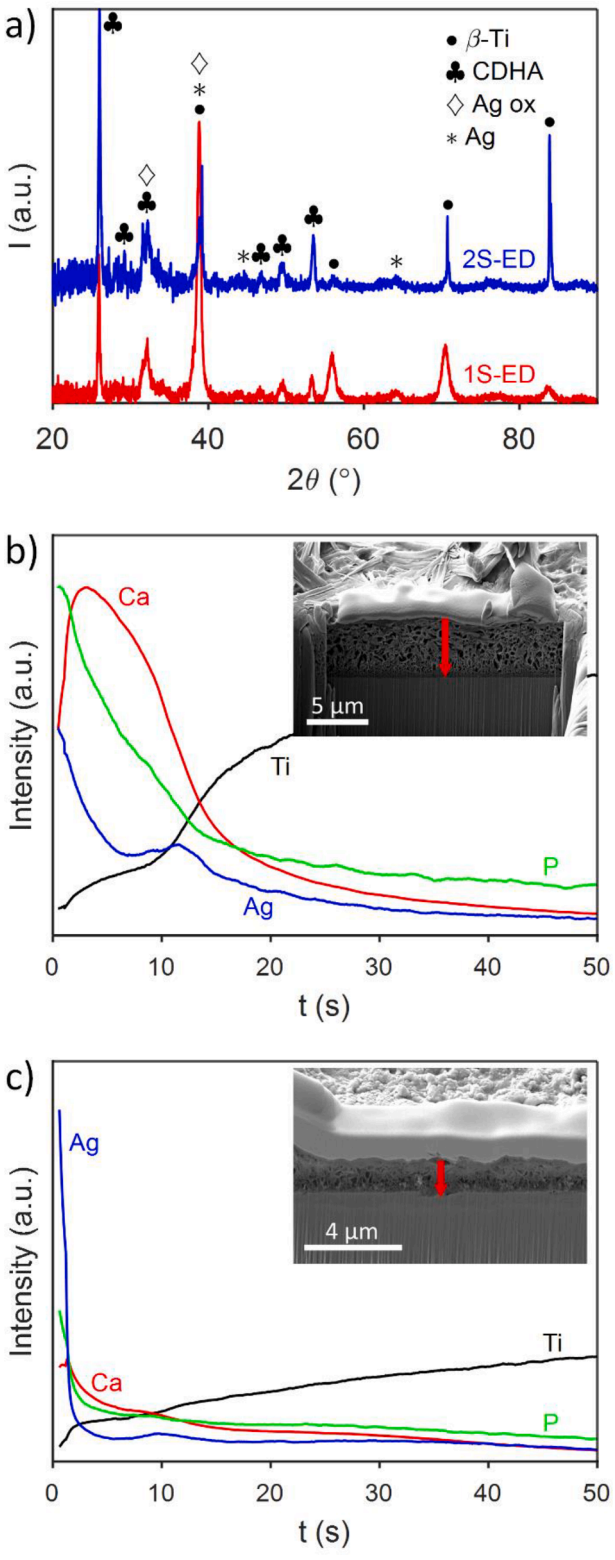

Fig 5. (a) GIXRD patterns of CDHA/AgNPs coatings grown by the 1S-ED at j_c = –2.7 mA/cm^2 followed by NaOH treatment, and 2S-ED at j = –20.76 mA/cm^2 (10 mM $AgNO_3$), (b) and (c) are the corresponding GDOES depth profiles. The insets show cross-section lamellae of the composite coatings and the red arrow the direction of the measurement.

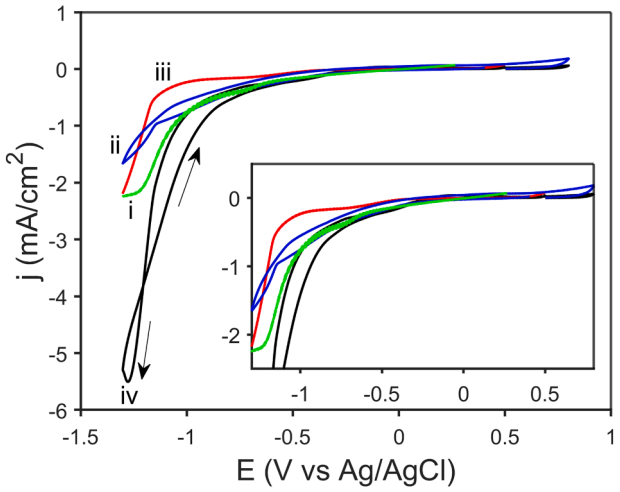

Fig. 6. (i) LSV on Ti-18Mo-6Nb-5Ta substrate and (ii) CV on glassy carbon from 42 mM $Ca(NO_3)_2{\cdot}4H_2O$ + 25 mM $NH_4H_2PO_4$ + 1 mM $Zn(NO_3)_2{\cdot}6H_2O$, (iii) LSV on Ti-18Mo-6Nb-5Ta substrate and (iv) CV on glassy carbon from 5 mM $Zn(NO_3)_2{\cdot}6H_2O$ + 5 mM KNO_3.

possibly attributed to Zn^{2+} reduction [29]. However, the concomitant reduction of nitrate ions is known to yield hydroxyl ions in solution (Eq. 1) that react with Zn^{2+} to form ZnO onto the electrode (Eq 2):

$$NO_3^{2-} + H_2O + 2e^- \rightarrow NO_2^- + 2OH^- \quad \text{(Eq. 1)}$$

$$Zn^{2+} + 2OH^- \rightarrow ZnO + H_2O \quad \text{(Eq. 2)}$$

In addition, since the electrolyte was not de-aerated, hydroxyl ions can also be electrogenerated from the oxygen dissolved in the electrolyte. The deposition of ZnO was delayed onto the β-Ti alloy compared to the glassy carbon electrode (cf. curves *iii* and *iv*). Pulse current electrodeposition was also chosen to produce Zn-containing composite coatings. For the 1S-ED approach, average current densities between –1.3 and –5.3 mA/cm^2 were applied, while for the 2S-ED approach, deposition of ZnO onto the previously grown CDHA was carried out by DC at *j* between –1 and –4.4 mA/cm^2. The working temperature (70 °C) was selected on the basis of prior studies [30].

Fig. 7 shows the chemical composition of the resulting composite coatings. Similar trends regarding Ca/P ratio of the calcium phosphate matrix were observed. First, an increase with the post-alkaline treatment in the case of the 1S-ED derived coatings (Fig. 7a). The corresponding Zn content could be tuned from 4 wt% to 10 wt% depending on the applied j_c and the alkaline treatment (Fig. 7b). Interestingly, larger amounts of Zn could be detected in coatings produced by the 2S-ED approach (Fig. 7d), reaching 50 wt% at the j = –1 mA/cm^2 used to coat the CDHA matrix with Zn-based species.

The morphology of the Zn-containing coatings obtained from the two approaches was quite different. ZnO-NPs could not be identified in any of the samples obtained by the 1S-ED method (Fig. 8a), although EDX analyses indicated that the Zn element was present (not shown). In addition, the morphology of the CDHA matrix was seemingly different from that observed for Ag codeposition, suggesting that Zn could exert a doping role and had impacted the morphology of CDHA. This agrees with the homogeneous distribution of Zn across the sample surface and with the featureless LSV and CV curves of Fig. 6. Pulse galvanostatic deposition at j_c = –2.7 mA/cm^2 (t_{on} = 1s and t_{off} = 1s, 177 cycles) on the β-Ti alloy from 1 mM $Zn(NO_3)_2{\cdot}6H_2O$ indicated that ZnO nanoparticles grew on it (Fig. S3), but the same features could not be found in the composite.

On the other hand, aggregates of tiny particles were easily found in coatings obtained by the 2S-ED approach (Fig. 8b). The corresponding EDX patterns showed the presence of Zn (Fig. 8c) and the XRD spectrum display reflections that match the hexagonal ZnO phase (PDF 074-0534)

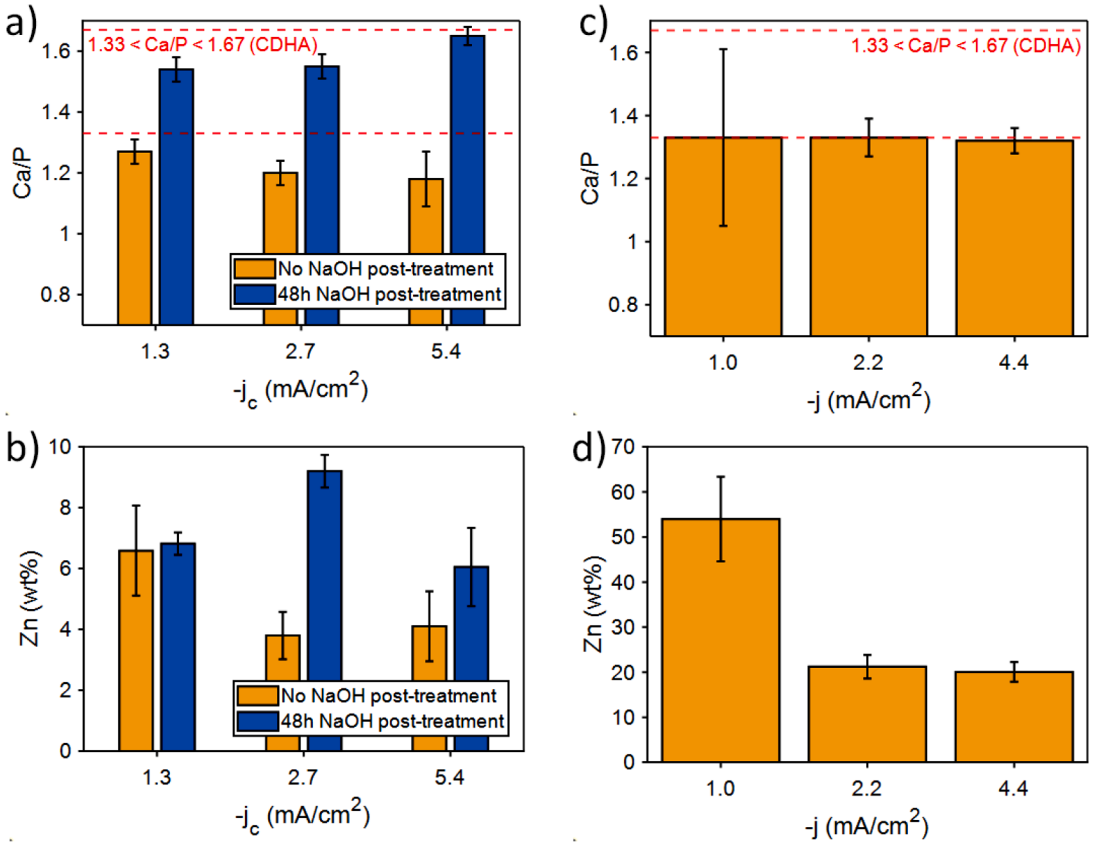

Fig. 7. Compositional analysis of (a,b) Zn-containing CDHA coatings obtained by 1S-ED approach: (a) Ca/P ratio and (b) Zn wt% for coatings produced at the indicated j_c both before and after the NaOH treatment. Compositional analysis of (c,d) coatings obtained by 2S-ED approach: (c) Ca/P ratio and (d) wt% Zn in coatings produced at the indicated j on top of the CDHA. Note that the y-axis in panel d) is different from b).

(Fig. 8d). The E-t curves recorded during the deposition of ZnO on the CDHA-coated β-Ti alloy are shown in Fig. S4, Supplementary Information. A potential shift towards more negative values is observed as the applied current density is made more negative. Finally, Fig. S5 shows the SEM and EBS images of a composite coating with the highest Zn content according to Fig. 7d. The presence of small hexagonal-shaped rods typical of hexagonal ZnO can be appreciated, even forming a layer on top of the CDHA matrix. FIB-SEM cross-sections of the ZnO/CDHA composites were also imaged and the corresponding thicknesses were determined. Values of 2.8 μm and 2.0 μm were measured for the 1S- and 2S-ED coatings, respectively (Fig. S6). Again, the 2S-ED coatings were thinner, which we believe it can be explained by a partial dissolution of the already deposited CDHA layer during the deposition of Ag and ZnO.

4. Conclusions

The electrodeposition of Ag- and Zn-containing CDHA composites can be successfully accomplished from either a single electrolyte or two electrolytes (i.e., two consecutive electrodeposition processes). Under optimized conditions, the latter approach renders composites with well-defined and non-aggregated AgNPs, even in the absence of stabilizers in the electrolyte, which are located at the utmost surface of the previously grown CDHA layer. On the other hand, agglomerates of ZnO-NPs were found in coatings obtained by consecutive electrodeposition, at least within the window of explored conditions. The one-step approach still leads NPs for the Ag case, although the growth proceeds in a more dendritic fashion. In addition, the NPs are partly engulfed in the CDHA matrix, which can be beneficial in certain cases (e.g., for a more sustained release of Ag^+ ions). Meanwhile, no clear formation of NPs was found for Zn. The present study shows that composite coatings with varying content of antibacterial elements or compounds, aggregation degree, and location in the CDHA host can be modulated to a great extent by electrochemical means. The investigation of the impact of these variables on the antibiofilm and antibacterial performance of the coatings is in progress and will be furnished in a future study.

Funding

This work was supported by the European Union's Horizon 2020 research and innovation programme under the Marie Skłodowska-Curie grant agreement No. 861046 ('Bioremia' European Training Network), and from the Generalitat de Catalunya (2021-SGR-00651). Partial funding was also provided by the Spanish Goverrnment through PID2020-116844RB-C21. The authors thank Dr. Zeng Peng of ScopeM for their support & assistance in this work.

CRediT authorship contribution statement

Michael Escobar: Methodology, Investigation, Validation, Formal analysis, Visualization, Writing – review & editing. **Volker Hoffmann:** Investigation, Resources, Writing – review & editing. **Thomas Gemming:** Investigation, Resources, Writing – review & editing. **Minsoo Kim:** Investigation, Writing – review & editing. **Salvador Pané:** Resources, Writing – review & editing. **Jordi Sort:** Supervision, Funding acquisition, Conceptualization, Writing – review & editing. **Eva Pellicer:** Methodology, Formal analysis, Visualization, Supervision, Project administration, Conceptualization, Writing – original draft.

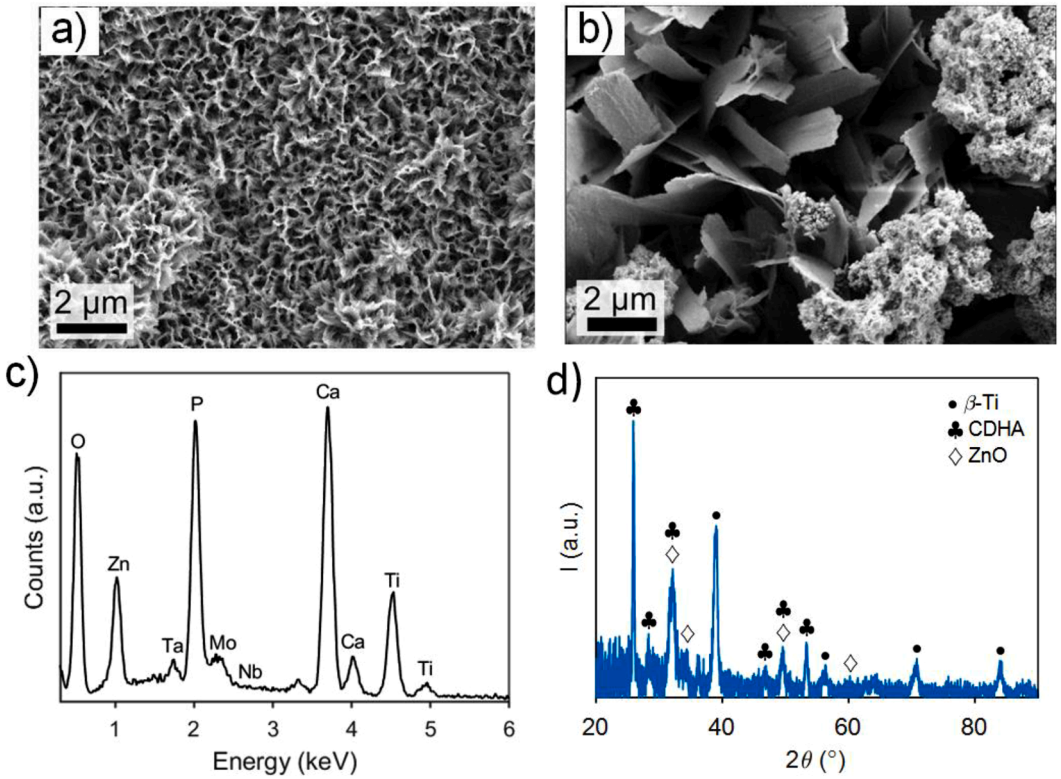

Fig. 8. (a) SEM image of Zn-containing CDHA coating deposited by the 1S-ED method at $j_c = -2.7$ mA/cm^2 followed by NaOH treatment, (b) SEM image of ZnO/CDHA coating deposited by the 2S-ED method at $j = -2.2$ mA/cm^2, (c, d) corresponding EDX and GIXRD patterns of the sample shown in (b).

Declaration of Competing Interest

The authors declare that they have no conflict of interest.

Data availability

Data will be made available on request.

Supplementary materials

Supplementary material associated with this article can be found, in the online version, at doi:10.1016/j.surfin.2023.103671.

References

[1] J. Yi, M.L. Li, H.X. Zhou, A. Rosenkranz, B. Wang, H. Song, N. Jiang, Enhanced tribological properties of Y/MoS_2 composite coatings prepared by chemical vapor deposition, Ceram. Int. 46 (2020) 23813–23819, https://doi.org/10.1016/j.ceramint.2020.06.157.

[2] R. Askarnia, M. Sobhani, M. Zare, H. Aghamohammadi, H. Staji, Incorporation of Al_2O_3 and ZrO_2 ceramics to AZ31 magnesium alloys composite coating using micro-arc oxidation method, J. Mech. Behav. Biomed. Mater. 141 (2023), 105784, https://doi.org/10.1016/j.jmbbm.2023.105784.

[3] A. Błoniarz, K. Cholewa-Kowalska, M. Gajewska, B. Grysakowski, T. Moskalewicz, Electrophoretic deposition, microstructure and selected properties of nanocrystalline SnO_2/Sr enriched bioactive glass/chitosan composite coatings on titanium, Surf. Coat. Technol. 450 (2022), 129004, https://doi.org/10.1016/j.surfcoat.2022.129004.

[4] A. Mulone, Z. Xia, U. Klement, Electrodeposition of FeW-graphene composites: effect of graphene oxide concentration on microstructure, hardness and corrosion properties, FlatChem 40 (2023), 100525, https://doi.org/10.1016/j.flatc.2023.100525.

[5] I. Gurrappa, L. Binder, Electrodeposition of nanostructured coatings and their characterization—a review, Sci. Technol. Adv. Mater. 9 (2008), 043001, https://doi.org/10.1088/1468-6996/9/4/043001.

[6] F.C. Walsh, S. Wang, N. Zhou, The electrodeposition of composite coatings: diversity, applications and challenges, Curr. Opin. Electrochem. 20 (2020) 8–19, https://doi.org/10.1016/j.coelec.2020.01.011.

[7] T.T. Li, L. Ling, M.C. Lin, H.K. Peng, H.T. Ren, C.W. Lou, J.H. Lin, Recent advances in multifunctional hydroxyapatite coating by electrochemical deposition, J. Mater. Sci. 55 (2020) 6352–6374, https://doi.org/10.1007/s10853-020-04467-z.

[8] N. Eliaz, N. Metoki, Calcium phosphate bioceramics: a review of their history, structure, properties, coating technologies and biomedical applications, Materials 10 (2017) 334, https://doi.org/10.3390/ma10040334.

[9] R. Drevet, H. Benhayoune, Electrodeposition of calcium phosphate coatings on metallic substrates for bone implant applications: a review, Coatings 12 (2022) 539, https://doi.org/10.3390/coatings12040539.

[10] T. Mokabber, L.Q. Lu, P. Van Rijn, A.I. Vakis, Y.T. Pei, Crystal growth mechanism of calcium phosphate coatings on titanium by electrochemical deposition, Surf. Coat. Technol. 334 (2018) 526–535, https://doi.org/10.1016/j.surfcoat.2017.12.011.

[11] A. Vladescu, D.M. Vranceanu, S. Kulesza, A.N. Ivanov, M. Bramowicz, A. S. Fedonnikov, M. Braic, I.A. Norkin, A. Koptyug, M.O. Kurtukova, M. Dinu, I. Pana, M.A. Surmeneva, R.A. Surmenev, C.M. Cotrut, Influence of the electrolyte's pH on the properties of electrochemically deposited hydroxyapatite coating on additively manufactured Ti64 alloy, Sci. Rep. 7 (2017) 16819, https://doi.org/10.1038/s41598-017-16985-z.

[12] X. Chen, J. Zhou, Y. Qian, L. Zhao, Antibacterial coatings on orthopedic implants, Mater. Today Bio 19 (2023), 100586, https://doi.org/10.1016/j.mtbio.2023.100586.

[13] T. Mokabber, H.T. Cao, N. Norouzi, P. Van Rijn, Y.T. Pei, Antimicrobial electrodeposited silver-containing calcium phosphate coatings, ACS Appl. Mater. Interfaces 12 (2020) 5531–5541, https://doi.org/10.1021/acsami.9b20158.

[14] B. Maimaiti, N. Zhang, L. Yan, J. Luo, C. Xie, Y. Wang, C. Ma, T. Ye, Stable ZnO-doped hydroxyapatite nanocoating for anti-infection and osteogenic on titanium, Colloids Surf. B 186 (2020), 110731, https://doi.org/10.1016/j.colsurfb.2019.110731.

[15] R. Ghosh, O. Swart, S. Westgate, B.L. Miller, M.Z. Yates, Antibacterial copper–hydroxyapatite composite coatings via electrochemical synthesis, Langmuir 35 (2019) 5957–5966, https://doi.org/10.1021/acs.langmuir.9b00919.

[16] X. Lu, B. Zhang, Y. Wang, X. Zhou, J. Weng, S. Qu, B. Feng, F. Watari, Y. Ding, Y. Leng, Nano-Ag-loaded hydroxyapatite coatings on titanium surfaces by electrochemical deposition, J. R. Soc. Interface 8 (2011) 529–539, https://doi.org/10.1098/rsif.2010.0366.

[17] C.M. Xie, X. Lu, K.F. Wang, F.Z. Meng, O. Jiang, H.P. Zhang, W. Zhi, L.M. Fang, Silver nanoparticles and growth factors incorporated hydroxyapatite coatings on metallic implant surfaces for enhancement of osteoinductivity and antibacterial properties, ACS Appl. Mater. Interfaces 6 (2014) 8580–8589, https://doi.org/10.1021/am501428e.

[18] C. Fu, X. Zhang, K. Savino, P. Gabrys, Y. Gao, W. Chaimayo, B.L. Miller, M.Z. Yates, Antimicrobial silver-hydroxyapatite composite coatings through two-stage

electrochemical synthesis, Surf. Coat. Technol. 301 (2016) 13–19, https://doi.org/10.1016/j.surfcoat.2016.03.010.
[19] M.M. Fathy Abo-Elmahasen, A.S. Abo Dena, M. Zhran, S.A.H. Albohy, Do silver/hydroxyapatite and zinc oxide nano-coatings improve inflammation around titanium orthodontic mini-screws? *In vitro* study, Int. Orthod. 21 (2023), 100711, https://doi.org/10.1016/j.ortho.2022.100711.
[20] L.E. Valenti, L.V. Bonnet, M.R. Galiano, C.E. Giacomelli, A simple strategy to prepare hybrid coating on titanium (Ti6Al4V), Surf. Coat. Technol. 431 (2022), 128017, https://doi.org/10.1016/j.surfcoat.2021.128017.
[21] A. Mehrvarz, J. Khalil-Allafi, A. Motallebzadeh, V. Khalili, The effect of ZnO nanoparticles on nanomechanical behavior of Hydroxyapatite electrodeposited on NiTi biomedical alloy, Ceram. Int. 48 (2022) 35039–35049, https://doi.org/10.1016/j.ceramint.2022.08.093.
[22] Y. Huang, H. Zeng, X. Wang, D. Wang, Corrosion resistance and biocompatibility of SrHAp/ZnO composite implant coating on titanium, Appl. Surf. Sci. 290 (2014) 353–358, https://doi.org/10.1016/j.apsusc.2013.11.082.
[23] M. Escobar, O. Careta, N. Fernández Navas, A. Bartkowska, L.A. Alberta, J. Fornell, P. Solsona, T. Gemming, A. Gebert, E. Ibáñez, A. Blanquer, C. Nogués, J. Sort, E. Pellicer, Surface modified β-Ti-18Mo-6Nb-5Ta (wt%) alloy for bone implant applications: composite characterization and cytocompatibility assessment, J. Funct. Biomater. 14 (2023) 94, https://doi.org/10.3390/jfb14020094.
[24] M.S. Safavi, F.C. Walsh, M.A. Surmeneva, R.A. Surmenev, J. Khalil-Allafi, Electrodeposited hydroxyapatite-based biocoatings: recent progress and future challenges, Coatings 11 (2021) 110, https://doi.org/10.3390/coatings11010110.
[25] R. Sivasubramanian, M.V. Sangaranarayanan, Electrodeposition of silver nanostructures: from polygons to dendrites, CrystEngComm 15 (2013) 2052, https://doi.org/10.1039/c3ce26886a.
[26] M. Naseri, M. Mohammadniaei, K. Ghosh, S. Sarkar, R. Sankar, S. Mukherjee, S. Pal, E. Ansari Dezfouli, A. Halder, J. Qiao, N. Bhattacharyya, Y. Sun, A robust electrochemical sensor based on butterfly-shaped silver nanostructure for concurrent quantification of heavy metals in water samples, Electroanalysis 35 (2023), e202200114, https://doi.org/10.1002/elan.202200114.
[27] N. Horiuchi, K. Madokoro, K. Nozaki, M. Nakamura, K. Katayama, A. Nagai, K. Yamashita, Electrical conductivity of polycrystalline hydroxyapatite and its application to electret formation, Solid State Ion. 315 (2018) 19–25, https://doi.org/10.1016/j.ssi.2017.11.029.
[28] V. Hoffmann, M. Hecker, R. Hübner, Focussing and defocussing effects at radio frequency glow discharge optical emission spectroscopy analyses of thin films with partly nonconductive components, Int. J. Mater. Res. 96 (2022) 983–987, https://doi.org/10.1515/ijmr-2005-0171.
[29] M.R. Khelladi, L. Mentar, M. Boubatra, A. Azizi, Study of nucleation and growth process of electrochemically synthesized ZnO nanostructures, Mater. Lett. 67 (2012) 331–333, https://doi.org/10.1016/j.matlet.2011.09.098.
[30] Y. Lghazi, J. Bahar, B. Youbi, M.A. Himi, C. Elhaimer, A. Elouadrhiri, I. Bimaghra, M. Ouknin, L. Majidi, Nucleation/growth and optical proprieties of Co-doped ZnO electrodeposited on ITO substrate, Biointerface Res. Appl. Chem. 12 (2021) 6776–6787, https://doi.org/10.33263/BRIAC125.67766787.